ACS OMEGA

http://pubs.acs.org/journal/acsodf

Article

Synthesis of Nickel Oxide Nanoparticles and Copper-Doped Nickel Oxide Nanocomposites Using *Phytolacca dodecandra* L'Herit Leaf Extract and Evaluation of Its Antioxidant and Photocatalytic Activities

Soruma Gudina Firisa, Guta Gonfa Muleta, and Ahmed Awol Yimer*

Cite This: *ACS Omega* 2022, 7, 44720−44732

Read Online

ACCESS | Metrics & More | Article Recommendations

ABSTRACT: Nanotechnology research is emerging as cutting-edge technology, and nanoparticles (NPs) and nanocomposites (NCs) have played a significant role in the bioremediation and treatment of polluted water by organic and nonorganic materials. Nanoparticles produced by plant extracts are more stable and biocompatible in comparison with those produced by physical and chemical methods. This research focuses on the synthesis of NiO NPs and Cu−NiO NCs using *Phytolacca dodecandra* L'Herit (P.d) leaf extract and evaluation of their antioxidant and photocatalytic activities. Cu−NiO NCs were synthesized using 50 mL of 0.1 M nickel(II) nitrate hexahydrate, 10 mL of 0.1 M copper(II) nitrate trihydrate, and 20 mL of leaf extract. The synthesized nanoparticles were characterized by UV−vis, X-ray diffraction (XRD), Fourier-transform infrared spectroscopy (FT-IR), and scanning electron microscopy (SEM) analyses to study the energy band gap, average crystallite size, functional groups, and morphology of the samples, respectively. The UV−vis analysis showed a red shift after copper doping, indicating a decrease in the optical band gap values. FT-IR characterization confirms the presence of various functional groups in samples. Crystallite sizes of the formed particles were obtained to be 14.18 and 16.10 nm from the XRD data for NiO NPs and Cu−NiO NCs, respectively. SEM showed the crystallinity of particles with a cubic structure. The photocatalytic degradation of methylene blue (MB) was found to be 78.3 and 97.8% by NiO NPs and Cu−NiO NCs, respectively. In the antioxidant test, NiO NPs and Cu−NiO NCs prevented the oxidation of 50% of the H_2O_2 molecules at a concentration of 363.96 and 350.29 μg/mL, respectively. Finally, the synthesized samples showed good photocatalytic and antioxidant activities.

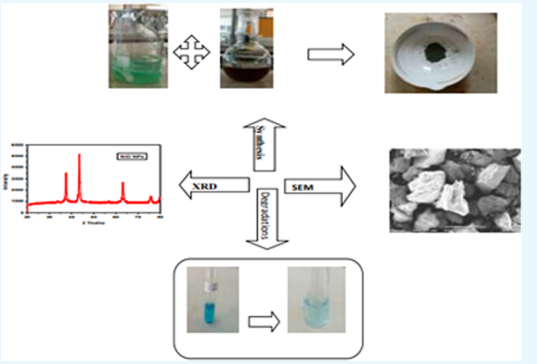

1. INTRODUCTION

Water pollution is a global challenge that has increased in both developed and developing countries. It affects economic growth as well as the socio-environmental sustainability and health of billions of people. It is elevated in international and national priorities.[1] Dyes form one of the most important classes of pollutants that result in colored wastewater that are sometimes hard to degrade because of their complex structure. Dye-containing wastewater is generated from the textile, tannery, dying, pulp and paper, and paint industries. The majority of dyes arise from dyeing and finishing processes in textile industries. Dye pollutants result in several health hazards such as skin- and eye-related diseases. Most dyes are toxic and pose a threat to aquatic living organisms.[2]

To comply with strict environmental regulations, several conventional methods such as adsorption, membrane processes, biological processes, and electrocoagulation have been utilized for the removal of dyes from water and wastewater. Conventional oxidation processes do not oxidize dyestuff with complex structures, and thus advanced oxidation processes are introduced for dye degradation.[3] There are many methods for degradation of dyes in wastewater including physical, chemical, and biological approaches, but degradation and maintenance costs of most of these methods are high and some of these processes will produce a secondary waste product that needs further treatment, so using them for the treatment of wastewaters is not suitable and economical.[2]

Antioxidants are molecules that can safely interact with free radicals, terminate the chain reaction, and convert them to a harmless molecule by donating an electron. In the last decade, antioxidants have attracted attention due to their potential to

Received: June 28, 2022
Accepted: November 4, 2022
Published: December 1, 2022

minimize oxidative stress, which is defined as the pathophysiological response created due to the imbalance between the production of oxidants and the endogenous antioxidants that work against it. Hence, there is a net increase of the reactive oxygen species (ROS) including superoxide anions, hydroxyl radicals ($HO^{\bullet}$), hydrogen peroxide (H_2O_2), singlet oxygen ($^1O_2$), and reactive nitrogen species (RNS) (e.g., peroxynitrite, peroxyl radicals). Free radicals with various chemical origins are very unstable, and they extract electrons from other molecules to reach equilibrium, leading to the degradation of the target molecule. By scavenging free radicals, the harmful effects of free radicals such as cancer, heart disease, and neurodegenerative disorders may be minimized. As a result, there is a pressing need to devise some practical means of dealing with these serious diseases.[4] Inorganic nanoparticles are thermally stable and chemically inert, which facilitate exploiting the potential, as well as the immobilization of natural antioxidants. Moreover, nanoparticle-conjugated natural antioxidants facilitate chemical stability of the antioxidants in physiological conditions, deliver the product in intact molecular form in a wider concentration range, and most importantly enable slow and continuous release.[5]

Among metal oxide NPs, NiO NPs are capable of scavenging the ROS with high capability. NiO NPs synthesized by a facile green combustion method using *Limonia acidissima* natural fruit juice show a significant hydroxyl radical scavenging activity.[6] Biosynthesized NiO NPs synthesized using *Raphanus sativus* extract and calcined at 100 °C had the best antioxidant potential with an IC_{50} of 258 g/mL.[7]

Nanoparticles have played a significant role in the bioremediation and treatment of polluted water by organic and nonorganic materials.[2] There are three fundamental practices for nanoparticle synthesis such as chemical, biological, and physical approaches. Chemical and physical methods require more investment and consume more time, which likely results in toxic final products. Hence, the nontoxic and least expensive natural (biological) methodology was picked for nanoparticles synthesis. Compared to other methods, the biological approach is eco-friendly. Most of the time, the source for this approach was plant parts. The nanoparticles produced by plant extracts are more stable and biocompatible in comparison with those produced by physical and chemical methods.[8] In recent research, NiO NPs have drawn considerable interest because of their unique properties, such as large surface-area-to-volume ratios, low porosity, high dispersion rates, high photoabsorption, and small heat capacities. Since the particle size, morphology, and high crystallinity influence the physicochemical properties, it is of great importance to synthesize NiO NPs with a small particle size, which could enhance the efficiency of their applications. These unique properties of NiO NPs make their viable and cost-effective surfaces suitable for different applications such as in adsorbents, solar fuel cells, catalytic agents, gas sensors, antibacterial materials, and hydrogen storage.[4,5]

Biological methods of synthesis of NPs using microorganisms such as algae, fungi, bacteria, and plant leaf extracts have been suggested as possible eco-friendly alternatives to chemical methods as these methods are low-cost, energy-efficient, and nontoxic.[9,10] The advantage of using plants for the synthesis of NPs is that they are easily available, safe to handle, and possess a broad variability of metabolites that may aid in reduction. Based on previous literature reports, NiO NPs were synthesized from various plant extracts such as Sageretia thea (Osbeck.) and Stevia leaf extract,[11,12] and their antioxidant activities were also reported. And the results found are quite conclusive. However, we found that there is no report on the synthesis of NiO NPs and copper-doped NiO NCs using *Phytolacca dodecandra* L'Herit leaf extract.

In the present study, *P. dodecandra* L'Herit leaf extracts were considered for the synthesis of nanoparticles as this is the first ever detailed report on the plant being utilized for green synthesis of NiO NPs and Cu−NiO NCs. *P. dodecandra* L'Herit is native to sub-Saharan Africa and Madagascar. It is a member of the Phytolaccaceae family and is commonly known in Ethiopia as "endod." Other local names include soapberry and African soapberry (English). The plant is a sprawling woody climber with an average length of stems that reaches 5−8 m. It grows rapidly especially during the rainy season with erect, racemic, dioecious flowering stalks and red berries. Previous phytochemical investigations on this plant revealed that the *P. dodecandra* L'Herit leaves are rich in various secondary metabolites like alkaloids, proteins and amino acids, saponins, flavonoids, terpenoids, and total phenols and tannins.[9]

The facile synthesis of NiO NPs and Cu−NiO NCs is reported using the leaf extract of *P. dodecandra* L'Herit as a reducing and stabilizing agent. The effects of various reaction parameters affecting the synthesis of NPs were also studied. The physicochemical characteristics were investigated, the structure and phase distributions of the obtained samples were determined by X-ray diffraction (XRD), the nanocomposite morphology was analyzed by scanning electron microscopy (SEM), the optical band gap was obtained from UV−visible spectroscopy (UV−vis), and the presence of various functional groups present in samples was analyzed by Fourier transform infrared (FT-IR) spectroscopy. Moreover, the photocatalytic and antioxidant activities of the synthesized samples were investigated.

2. MATERIALS AND METHODS

2.1. Materials. Nickel nitrate hexahydrate, methylene blue, hydrogen peroxide, sodium hydroxide, phosphate buffer, sulfuric acid, nitric acid, chloroform, Wagner's solution, ferric chloride, concentrated hydrochloric acid, ascorbic acid, distilled water, and *P. dodecandra* L'Herit leaves were used. All chemicals and reagents used in this study were of analytical grade.

2.2. Sample Collection and Preparation. The *P. dodecandra* L'Herit (P.d) leaves were collected by a random sampling technique from the Jimma University Garden, Jimma, Southwest Ethiopia, and thoroughly washed with tap water to remove debris and other contaminants, followed by wasing with distilled water and air-dried at room temperature. The dried sample was ground with a mortar and pestle, and then, the aqueous extract of the leaf was prepared by boiling 10 g of the leaves with 100 mL of distilled water at about 60 °C for 20 min.[13,14] The extract was cooled to room temperature and filtered using Whatman No. 1 filter paper. Finally, the extract was stored to be used for further experiments.[8]

2.3. Phytochemical Test of *P. dodecandra* L'Herit Leaf Extract. *2.3.1. Test for Flavonoids. 2.3.1.1. Alkaline Reagent Test.* The extract (1 mL) was treated with 5 mL of NaOH. The presence of flavonoids was confirmed by the formation of the intense yellow color.[15]

2.3.2. Test for Alkaloids. 2.3.2.1. Wagner's Test. The solvent extract (1 mL) was acidified with 1 mL of 1.5% v/v of

https://doi.org/10.1021/acsomega.2c04042
ACS Omega 2022, 7, 44720−44732

HCl, and 1 mL of Wagner's reagent was added. The occurrence of alkaloids was indicated by the formation of yellow and/or brown precipitates.[16]

2.3.3. Test for Saponins. 2.3.3.1. Frothing Test. About 1 mL of the extract was diluted separately with 20 mL of distilled water and was shaken in a graduated cylinder for 15 min. A 1 cm layer of foam was formed, which indicates the presence of saponins.[15]

2.3.4. Test for Tannins and Phenolic Compounds. 2.3.4.1. Ferric Chloride Test. The extract (1 mL) was treated with a few mL of 5% neutral ferric chloride. The formation of a dark blue and/or bluish-black color product showed the presence of tannins and phenol.[15,16]

2.4. Synthesis of Nickel Oxide Nanoparticles. Green synthesis of the NiO NPs was carried out according to Ahmad et al.[1717] with minor modifications. For the synthesis of NiO NPs, 50 mL of 0.1 M nickel(II) nitrate hexahydrate ($Ni(NO_3)_2{\cdot}6H_2O$) was stirred for 20 min; then, 20 mL of leaf extract was added dropwise. The mixture was progressively stirred for 30 min at room temperature using a magnetic stirrer with a stirring speed of 4000 rpm. The pH of the solution was adjusted by adding 5 M NaOH drop by drop until the pH of the solution reached 10. The resultant mixture was stirred at room temperature for 2 h, and the obtained precipitate was centrifuged for 10 min, followed by washing with distilled water and ethanol several times to remove impurities and dried at 70 °C for 2 h in an oven. Finally, the dried powder was calcinated in a muffle furnace for 2 h at 400 °C. The product was used for further studies.

2.5. Synthesis of Copper-Doped Nickel Oxide Nanocomposites. The Cu-doped NiO photocatalyst was synthesized according to Ahmad et al.[17] with some modifications. In a typical procedure, 50 mL of 0.1 M nickel(II) nitrate hexahydrate ($Ni(NO_3)_2.6H_2O$) and 10 mL of 0.1 M copper(II) nitrate trihydrate $Cu(NO_3)_2.3H_20$ were added dropwise into 20 mL of leaf extract to prepare the Cu−NiO catalyst. The mixed solution was then stirred for 30 min at room temperature using a magnetic stirrer with a stirring speed of 4000 rpm and a reaction time of 30 min. Then, 5 M NaOH was added drop by drop until the pH of the solution reached 10. The resultant mixture was stirred at room temperature for 2 h, and the precipitate was centrifuged and washed with distilled water and ethanol to remove the impurities and then dried in an oven at 70 °C for 2 h. The resulting powder was calcined at 400 °C for 2 h according to the literature reported.[16] The resultant powder was used for further studies.

2.6. Physicochemical Methods of Characterization. The electronic spectra of the NiO NPs and Cu−NiO NCs in solution were run in the range of 300−800 nm on a 6705 UV/vis spectrophotometer (jenway). The analysis was carried out with quartz cuvettes as sample containers. The reaction mixture was monitored spectrophotometrically. Generally, the surface plasmon resonance of the synthesized nanoparticles and the energy band gap of the synthesized samples were analyzed by UV−vis spectroscopy. FT-IR spectroscopy was used to determine the vibrational frequency of stretching and bending modes of the molecules as well as possible biomolecules, which are responsible for the reduction and capping of NPs. For the FT-IR analysis, the prepared samples were dried and ground with KBr pellets and analyzed on a FT-IR spectrophotometer (PerkinElmer Frontier). Fourier transform infrared (FT-IR) spectra were recorded in the scanning range of 4000−400 cm^{-1}. In FT-IR analysis, the samples were mixed with solid KBr uniformly and properly, which was compressed to settle down on a thin transparent film, and this thin transparent film was kept in the chamber of the instrument for scanning. FT-IR analysis was used to identify the presence of functional groups and to receive valuable information regarding the presence of ligands in the metal NPs as KBr disks on a PerkinElmer. The X-ray diffraction (XRD) spectrum was used to confirm the crystalline nature of the synthesized NiO NPs and Cu−NiO NCs. The powdered sample was placed on a glass slide and subjected to computer-controlled XRD analysis. The crystallinity and crystalline phase of the synthesized samples were determined through X-ray diffraction (XRD) profiles (DR AWELL XRD-700) using 2Cu Kα radiation (λ = 1.54Å) in the 2θ range of 20−80 with a scan speed of 0.03°/min, and the average particle size was also calculated from the diffractogram using the Debye−Scherrer formula.

$$D = k\lambda/\beta\cos\theta$$

where D is the crystallite size, k = 0.9, λ is the X-ray source wavelength, β is the full width at half-maximum (FWHM) of a peak, and θ is the Bragg diffraction angle.

The morphological features of the prepared NiO NPs and Cu−NiO NCs were studied using scanning electron microscopy (SEM) (JCM-6000Plus). In SEM characterization, nanoparticle powder is mounted on a sample holder, followed by coating with a conductive metal. The sample is then scanned with a focused fine beam of electrons. The surface characteristics of the sample were obtained from the secondary electron emitted from the sample surface. Computer software was used to collect/analyze the resulting patterns to determine the crystallography of the material.

2.7. Photocatalytic Degradation of Dyes. To evaluate the photocatalytic performance of the as-prepared sample toward the degradation of the MB dye, 20 mg of the prepared samples (NiO nanoparticles or Cu−NiO nanocomposites) was dispersed in 100 mL of 10 ppm MB dye solution using sunlight irradiation as a source of light. The suspension was stirred in the dark for 30 min before exposing to sunlight to ensure adsorption/desorption equilibrium between the photocatalysts and dye solution. Then, the system was illuminated under sunlight with continuous stirring. Aliquots of 5 mL were collected at regular intervals of time and centrifuged for 3 min. The UV−vis absorbance of the centrifuged samples was then determined by a UV−vis spectrometer. The degradation of the blank was determined similarly. The percentage degradation was determined using the following equation

$$\%\ \text{degradation} = [(C_0 - C_t)/C_0] \times 100$$

where C_0 is the initial concentration of the dye and C_t is the concentration of the dye at any time t.[18]

2.8. Reusability Performance of the Nanoparticles/Nanocomposites. To study its recyclability, the optimized catalyst doses (0.06 g) of NPs were allowed to settle by centrifugation after the photocatalytic degradation for 120 min (10 mg/L). The recovered catalysts were then collected and reused two times under the same photodegradation conditions according to the literature.[3]

2.9. Antioxidant Activity. The hydrogen peroxide scavenging activity was determined according to the method of Patil et al.[19] Different concentrations of the synthesized particles (0.1 mL) and ascorbic acid (50−1000 μg/mL) were mixed with hydrogen peroxide (0.6 mL, 50 mM) prepared

https://doi.org/10.1021/acsomega.2c04042
ACS Omega 2022, 7, 44720−44732

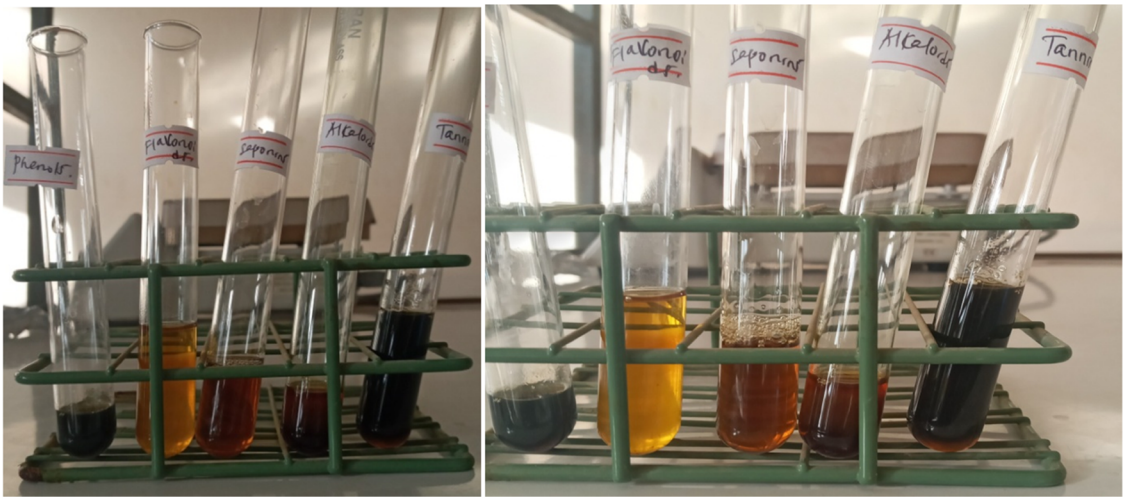

Figure 1. Photographic image taken during the phytochemical test of *P. dodecandra* L'Herit leaf extract.

with phosphate buffer (pH 7.4). This reaction mixture was incubated for 10 min. The absorbance was measured spectrophotometrically at 230 nm using phosphate buffer as a blank. The percent of hydrogen peroxide scavenging was calculated using the following equation:

$$\% \text{ scavenging activity } [H_2O_2] = [(A_0 - A_1)/A_0] \times 100$$

where A_0 is the absorbance of control and A_1 is the absorbance of the sample.[20,21]

3. RESULTS AND DISCUSSION

3.1. Phytochemical Analysis of *P. dodecandra* L'Herit Leaf Extract. The phytochemical test was conducted for justification of different types of bioactive compounds that appear in the *P. dodecandra* L'Herit leaf extract using a different type of chemical, and it is shown in Figure 1. Knowing the correlation between the phytoconstituents and the bioactivity of a plant is desirable for the synthesis of compounds with specific activities.

The *P. dodecandra* L'Herit plant leaf extract was made by a simple decoction method using distilled water. A red-colored extract was obtained. The most important bioactive constituents of the plants are summarized in Table 1. This result has a close agreement with the literature.[15,16]

Table 1. Phytochemical Screening of the Plant Extracts[a]

sl. no.	phytochemical	chemical tests	results
1	phenolic	ferric chloride	+
2	alkaloids	Wagner's test	+
3	saponins	frothing test	+
4	tannins	ferric chloride	+
5	flavonoids	alkaline reagent	+

[a]+ indicates the presence of phytochemicals.

3.2. Synthesis of Nanoparticles. *3.2.1. Synthesis of NiO NPs.* A green synthesis method was used to fabricate NiO NPs using aqueous leaf extract of *P. dodecandra* L'Herit. When the bright green color of nickel nitrate hexahydrate was added to the leaf extract, a brown color was observed, which confirms the formation of NiO NPs. The phytochemicals present in the plant extract act as the reducing agent to convert metal ions to their corresponding nanoparticles and simultaneously act as an effective capping agent to prevent the NP agglomerations as revealed by the literature.[22]

3.2.2. Synthesis Cu–NiO NCs. During the synthesis of Cu–NiO NCs, bright green nickel nitrate hexahydrate, blue copper nitrate trihydrate, and red-colored leaf extract were added together, and a deep green color was formed, which indicates the formation of Cu–NiO NCs. Phytochemicals present in the plant extract act as the reducing agent to convert metal ions to their corresponding nanoparticles and simultaneously act as an effective capping agent to prevent the NC agglomerations as stated in the literature.[22]

3.2.3. Optimization of Different Parameters. 3.2.3.1. Concentrations of the Precursor. The ratio of the concentration of the precursor must correspond to the volume of the plant extract used.[23] In this study, 50 mL of different precursor concentrations (0.05, 0.02, 0.03, 0.1, and 0.2 M) was reacted with 20 mL of leaf extracts, and 0.1 M was optimized because it gave a sharp peak, which shows the formation of nanoparticles since the intensity of the surface plasmon peak has direct proportionality with the concentrations of the synthesized nanoparticles in the solution.[24] The result obtained was in close agreement with a recent report,[25] and an increase in intensity suggests that more nanoparticles are formed.[26]

3.2.3.2. Varying Volumes of Extracts. The synthesis of NPs using plant extracts is mainly influenced by the type of biomolecule found in plant extracts and the volume used. The volume of plant extracts used in the synthesis of nanoparticles plays a significant role in the reduction of metal ions to reduced metal in terms of their oxidation number.[27] To identify the optimum volumes of plant extracts, different volumes (10, 20, 30, 40, and 50 mL) were reacted at a fixed volume of precursors. In this manner, 20 mL was taken as the optimum volume as it showed the smallest wavelength. This is attributed to phytochemicals present in the plant extract, which are responsible for the bioreduction and stabilization of the NPs[28] that react with the precursor.

3.2.3.3. Varying Reaction Times. The reaction time is essential to the synthesis and stability of nanoparticles.[29] The effect of reaction time was evaluated during the green synthesis of nanoparticles. Different reaction times of 20–180 min with a difference of 10 were adopted and 120 min was chosen as the optimum reaction time. With this reaction time, the intensity

https://doi.org/10.1021/acsomega.2c04042
ACS Omega 2022, 7, 44720–44732

of the UV−vis peak increased, which shows that all precursors reacted with the leaf extract and reduction in metal ions was completed.

3.2.3.4. Effect of pH. The pH was one of the factors that influenced the size, shape, and composition of nanoparticles.[30] The effect of pH on the formation of NiO NPs has been evaluated by UV−vis spectroscopic studies. The pH in aqueous media can highly influence the progress of the metal ion reduction reaction.[31] The role of pH on NP synthesis could be seen in its effect on the capping and stabilizing abilities and consequently the growth of the nanoparticles. The presence of the OH^- ion in an alkaline pH environment might enhance the reducing and stabilizing capabilities of the biomolecules in the leaf extract.[32]

To know the optimum pH value of NPs, the pH range from 5 to 11 was tested. At pH 10, a blue shift was observed that could be attributed to the decrease in the particle size. Therefore, pH 10 was identified as the optimum pH. Above pH 10, it was not possible to synthesize NiO NPs, which may be because the high OH ion concentration hindered the process.[32] The rate of formation of NiO NPs is higher in basic pH than in acidic pH. The formation of NiO NPs occurs rapidly in the basic pH; it may be due to the ionization of the phenolic group present in the extract. The slow rate of formation and aggregation of NiO NPs at acidic pH could be related to the electrostatic repulsion of anions present in the solution.[26]

3.2.3.5. Volume of the Dopant for Nanocomposites. The absorption peak of Cu−NiO NCs was also affected by the concentration of the dopant.[33] To see the effect of the dopant (Cu) on the synthesis of Cu−NiO NCs, different volumes of the dopant (0.1 M Cu $(NO)_2{\cdot}3H_2O$) were added to get the optimum volume of the reaction. They are 10% (5 mL), 20% (10 mL), 30% (15 mL), 40% (20 mL), and 60% (30 mL). Finally, 20% was determined to be the optimum since it gave a UV−vis absorbance value at the largest wavelength (red shift). Therefore, it is possible to form a large amount of highly dispersed NPs with small particle sizes using P.d leaf extracts efficiently both as a reducing and stabilizing agent.

3.3. Characterization of the Synthesized Samples. *3.3.1. Electronic Spectra of the Synthesized Nanoparticles.* The absorption maxima of the synthesized NiO NPs and Cu−NiO NCs were determined with a UV−visible spectrophotometer. Figure 2 displays the UV−visible spectra.

The UV−vis spectra of the NPs and NCs were recorded in the range of 300−700 nm at room temperature. The obtained NPs displayed the characteristic surface plasmon resonance (SPR) band in the spectral range of 350−356 nm. This was in line with a previous study[34] that reported the optimum absorbance of NiO NPs at 350 nm wavelength. The synthesized NiO and Cu−NiO NCs showed maximum UV−vis absorbance at 350 and 356 nm, respectively, as shown in Figure 2. This figure is consistent with a recently reported study.[35]

The Tauc plot is shown in Figure 3. The optical band gap for the absorption peak is obtained by extrapolating the linear portion of $(\alpha h\nu)^2$ versus $h\nu$ to zero. Eg was found to be 3.19 and 2.85 eV for NiO NPs and copper-doped NiO NCs, respectively. The Cu−NiO NCs exhibit a lower band gap energy than NiO NPs.

3.3.2. Fourier Transform Infrared (FT-IR) Spectroscopy. The FT-IR spectrum of the leaf extract showed multiple peak values, indicating the presence of phenols, alcohols, alkanes,

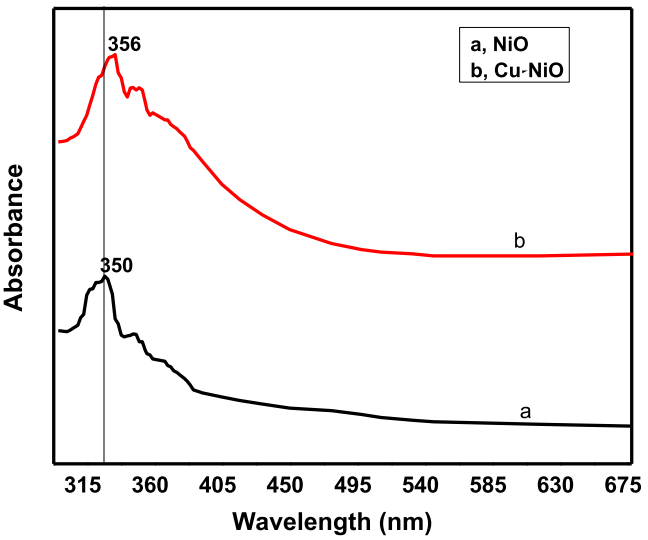

Figure 2. UV−vis spectra of NiO NPs and Cu−NiO NCs.

alkenes, aromatic compounds, carboxylic acids, and alkyl halides (Figure 4). The absence of peaks at 2220−2260 cm^{-1} indicated the absence of cyanide derivatives.[36] The absorption bands at 471 cm^{-1} are attributed to Ni−O vibrations[18] (Figure 5). In the case of Cu-doped NiO NCs, in addition to the 469 cm^{-1} peak, due to Ni−O stretching, the 631 cm^{-1} band was observed, which indicated the Cu−O stretching vibration band (Figure 5). The other peaks at 1051 cm^{-1} seen in the doped sample can be assigned to the different modes of Cu−O bond bending vibrations, which are in good agreement with the reported literature.[37]

From Figures 4 and 5, the very strong absorption band observed around 3400 cm^{-1} may be due to the presence of bonded N−H/C−H/O−H stretching of amines, amides, and alcohols. These peaks are consistent with the earlier reported spectra[38,39] because this plant leaf contains phenolic and alkaloid phytochemicals.

3.3.3. X-ray Diffraction (XRD) Analysis. The crystallinity and crystalline phase of synthesized samples were determined through X-ray diffraction (XRD) profiles (DRAWELL XRD −700 using 2Cu Kα radiation) in the 2θ range of 20 θ−80 θ with a scan speed of 0.03°/min. The XRD patterns of NiO NPs and Cu−NiO NCs are shown in Figure 6. The XRD pattern reveals the face-centered cubic-structured NiO. The Bragg peaks were obtained at 2θ values of 37.46, 43.51, 63.16, 75.65, and 79.71° corresponding to (111), (200), (202), (311), and (222), respectively. There were no other additional peaks throughout this diagram, which confirms the purity of obtained nanoparticles. The gathered data matched the standard pattern (JCPDS # 96-101-0096). All of the reflection can be indexed to the face-centered cubic NiO phase, similarly to recently reported works in the literature.[40,41]

The diffraction peaks are found to broaden with a decrease in their intensity as copper is doped in NiO, which may be a microstructural strain produced by the introduction of Cu^{+2} ions in the NiO lattice.[18] The crystallite size was found to increase with the doping of copper in nickel oxide due to the difference in the ionic radii of copper and nickel ions. It is clear from Figure 6 that no other characteristic peaks due to any impurities and sharp peaks are present in the pattern, indicating that the prepared samples are of high purity and crystallinity. The Bragg peaks were obtained at 2θ values of

https://doi.org/10.1021/acsomega.2c04042
ACS Omega 2022, 7, 44720−44732

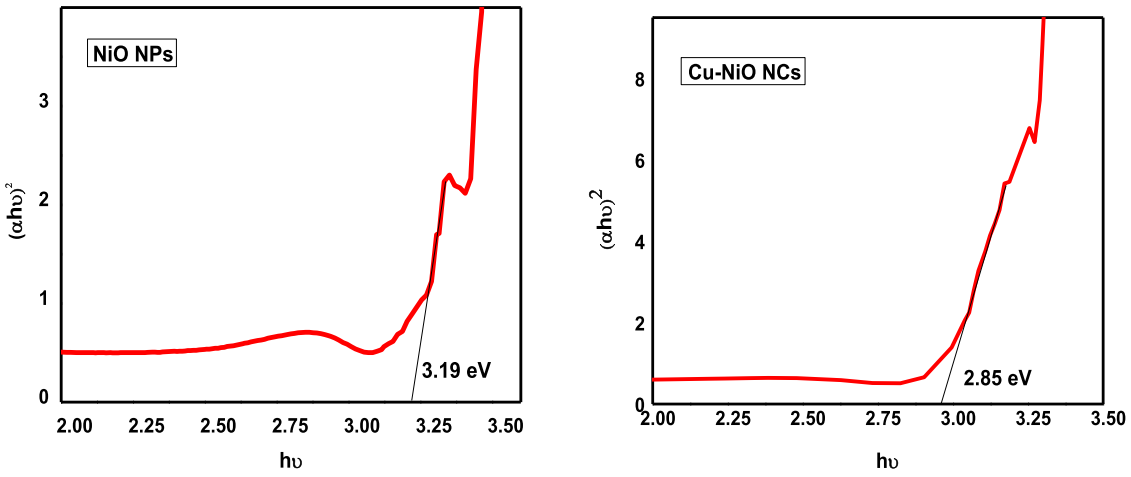

Figure 3. Calculated band gap of the synthesized nanoparticles.

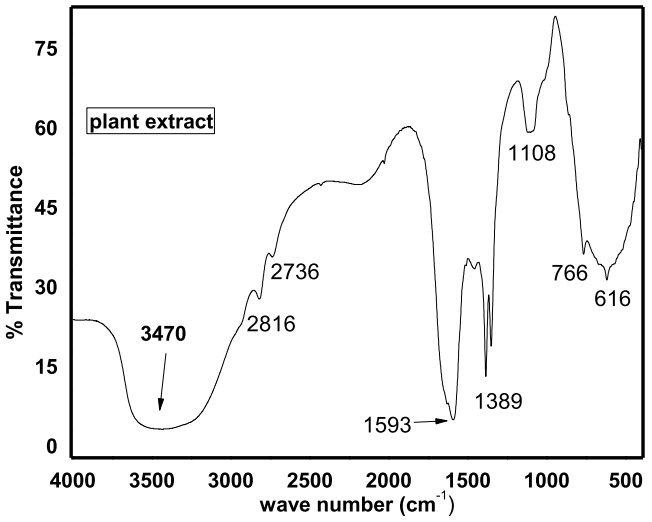

Figure 4. FT-IR spectrum of pure *P. dodecandra* L'Herit leaf extract.

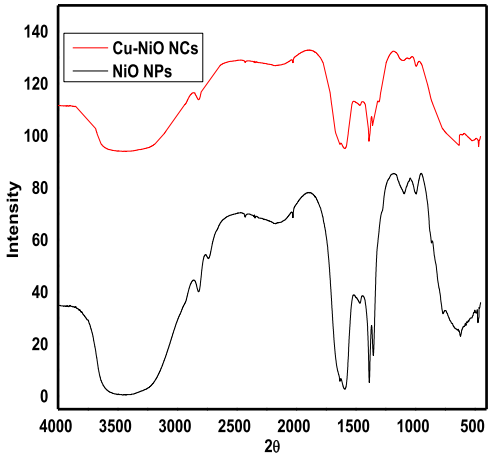

Figure 5. FT-IR spectra of the synthesized NiO NPs and Cu−NiO NCs.

35.74, 37.37, 43.35, 48.87, 62.96, 68.34, 75.28, and 79.51° corresponding to (11−1), (111), (200), (20−2), (202), (110), (311), and (222), respectively. The gathered data matched the standard pattern (JCPDS # 96-901-4581). The additional peaks obtained at 35.74, 48.87, and 68.34° correspond to

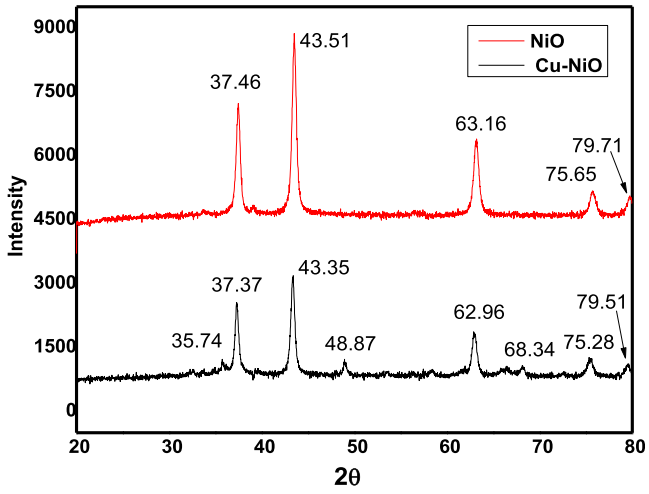

Figure 6. X-ray patterns of NiO NPs and Cu-NiO NCs.

copper; this is identical with the reported literature.[42] XRD of copper-doped NiO can have a pattern related to the presence of copper as revealed by the literature.[43]

The average sizes of the synthesized NiO NPs and Cu−NiO NCs calculated using the Scherrer formula from the data of the X-ray diffraction (XRD) pattern are 14.18 and 16.10 nm, respectively. The crystallite size was found to increase with the doping of Cu in NiO because the ionic radius of Cu is bigger than that of Ni (Cu = 0.082 nm > Ni = 0.078 nm).[44,45]

3.3.4. Scanning Electron Microscopy (SEM) Analysis. The surface morphological features of synthesized pure and doped NiO samples were studied by scanning electron microscopy; the images were recorded with magnifications of 1500, 1000, 500, and 50 (Figure 7). The SEM analysis indicates that the synthesized nanoparticles are appropriately dispersed and particles are cubical and highly crystalline (<10 nm); this is in good agreement with the reported literature.[46] Both the samples show nearly the same morphological features. Some of the synthesized nanoparticles are found to be agglomerated due to aggregation or overlapping of smaller particles, and they are essentially a cluster of nanoparticles, which is in close agreement with the result in the literature[47] that found an average size distribution of about 18 nm. It can be seen that pure NiO NPs reveal smaller-sized particles, while the doped sample shows comparatively large-sized particles. This result is

https://doi.org/10.1021/acsomega.2c04042
ACS Omega 2022, 7, 44720−44732

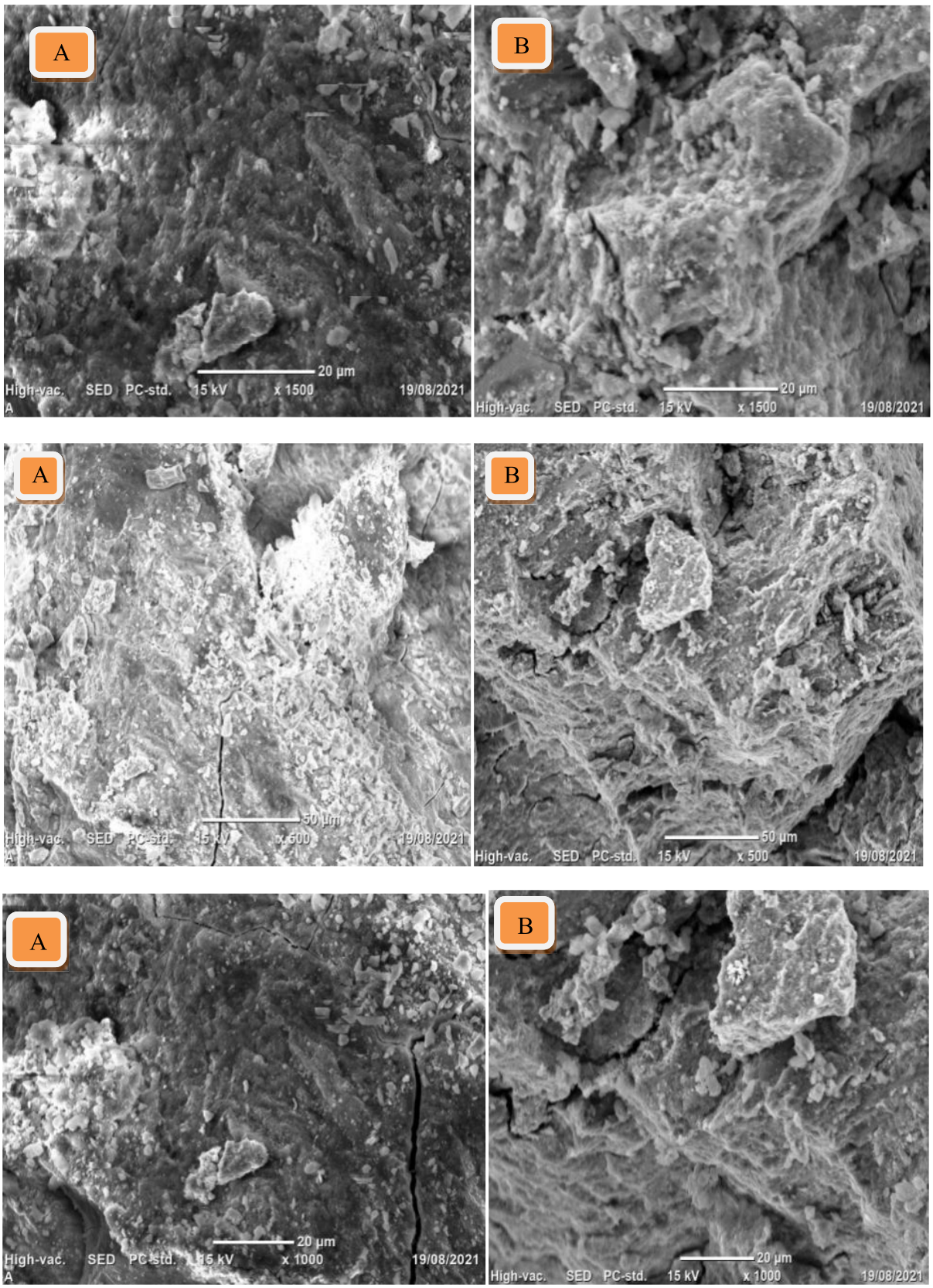

Figure 7. continued

https://doi.org/10.1021/acsomega.2c04042
ACS Omega 2022, 7, 44720−44732

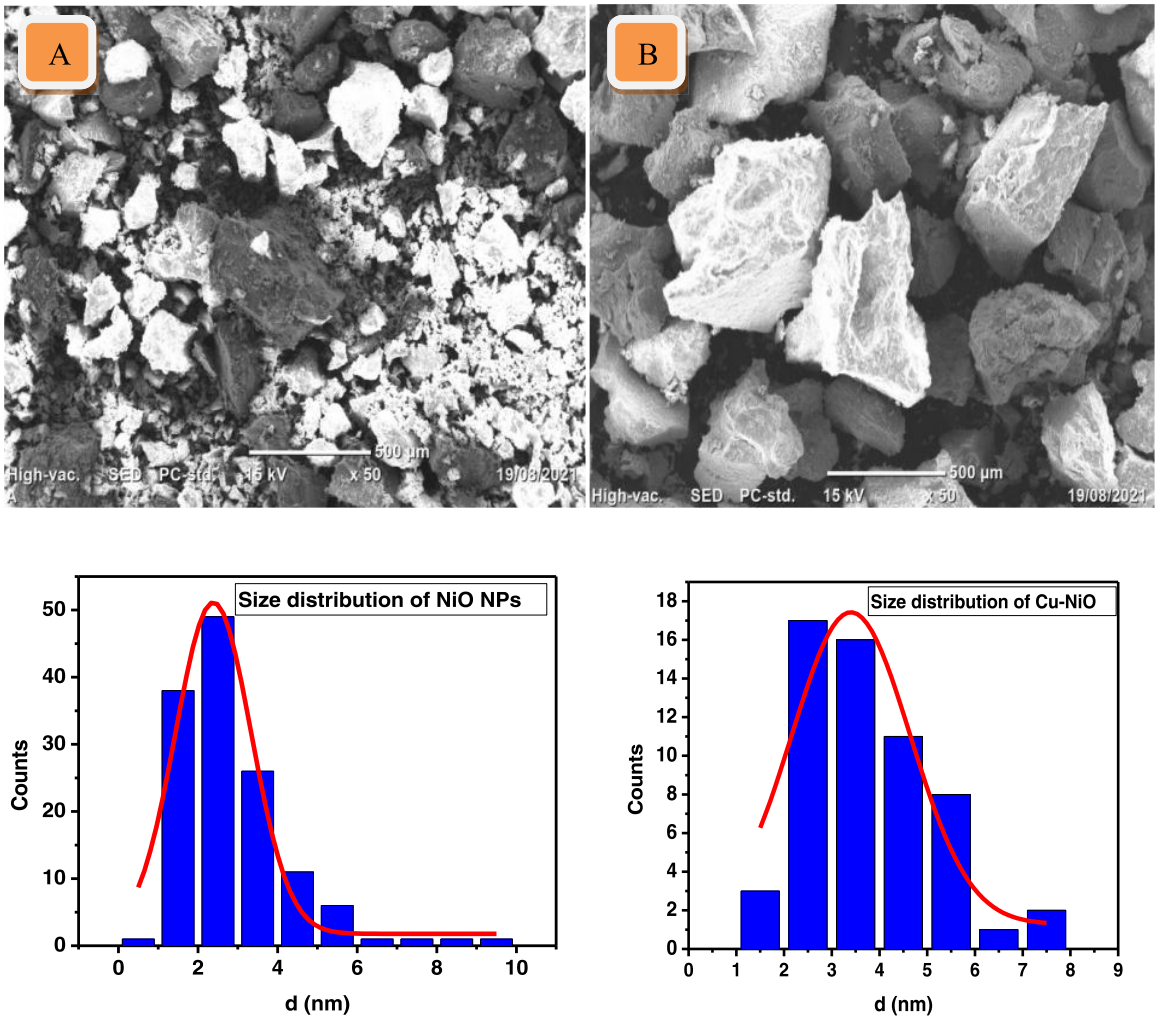

Figure 7. SEM images of NiO (A), Cu−NiO (B), and their size distributions (20 μm, 1000 mg).

in good agreement with the XRD data, which showed the formation of larger particle sizes in Cu-doped NiO NCs.

3.4. Photocatalytic Degradation of Dyes. *3.4.1. Effect of pH of the Solution.* The photocatalytic ability of the synthesized NiO NPs was analyzed against the different pH values of MB solution. The pH of the solution was adjusted using 0.1 M NaOH and 0.1 M HCl. The photocatalytic ability of the synthesized NiO NPs is directly proportional to the pH of the dye solution. Therefore, as the pH of the dye solution increases from 8 to 11, the degradation of the MB dye also increases (Figure 8). The reason here is that the variation of pH alters the surface properties of NiO NPs. The pHPZC (pH at point of zero charges) of Cu−NiO NCs was estimated to be 6.98. At pHPZC, catalysts have net-zero charges, and at pH < pHPZC, the surface of a catalyst becomes positively charged, whereas at pH > pHPZC, the surface is negatively charged. MB is a cationic dye; hence, at pH < pHPZC, it displayed a repulsive behavior due to the positively charged surface of the catalyst. Therefore, degradation proficiency decreases. When pH > pHPZC, the catalyst surface has a negative charge, which attracts the MB dye molecules to a greater extent.[6]

The experiment was carried out in the presence of NiO NPs and Cu−NiO NCs for an irradiation time of 160 min at 10 mg/L dye concentration, as shown in Figure 8. At pH 10, hydroxyl radicals are formed, leading to the formation of

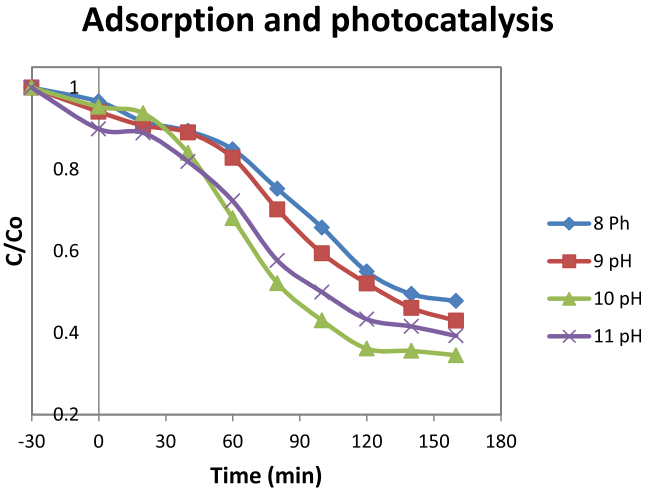

Figure 8. Effects of pH on MB removal with a catalyst.

hydrogen peroxide, which in turn results in an increase in hydroxyl radicals on a large scale. This increases the photocatalytic proficiency of catalysts under sunlight irradiation, and the degradation of the MB dye reaches up to 97.8%. At pH = 11, the surface of the catalyst becomes negatively charged by metal-bound OH^-; as a result, the adsorption of

https://doi.org/10.1021/acsomega.2c04042
ACS Omega 2022, 7, 44720−44732

MB molecules is hindered and they become less available for degradation due to the electrostatic repulsion between the surface charges on the adsorbate and the adsorbent, and so a decreased photocatalytic degradation efficiency is observed; this is in good agreement with a recently reported study.[13]

3.4.2. Effect of the Initial Dye Concentration. The effect of the dye concentration on the degradation ability of the catalyst was studied at an optimized pH and an irradiation time of 160 min by changing the initial dye concentration of 7, 10, and 13 mg/L. The MB solution containing NPs was kept in the dark for 30 min to achieve the adsorption−desorption equilibrium. The percent removal of MB solutions ranging from 7 and 10 to 13 mg/L was found to be around 10−15% after the 30 min adsorption in the dark. Then, it was followed by photocatalytic degradation under UV−vis light irradiation by assuming the time t = 0. Figure 9 clearly shows that the degradation

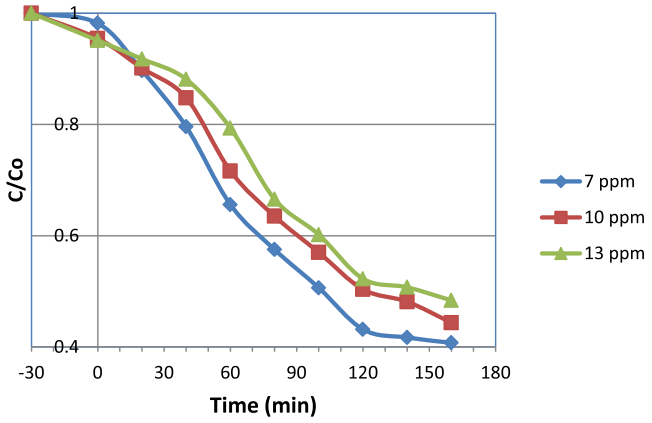

Figure 9. Effects of the initial dye concentration on photocatalytic degradation.

proficiency of the catalyst is inversely related to the initial dye concentration of the MB dye. As the initial dye concentration of MB increases, the time needed for complete degradation increases and photocatalytic proficiency decreases. At a high concentration of a dye, maximum number of dye molecules are adsorbed on the catalyst surface, resulting in reduced light penetration. Due to fewer hydroxyls, the photocatalytic activity diminished; this is also reported in the literature.[3]

3.4.3. Effect of Irradiation Time. The reaction kinetics depends on the irradiation time; hence, a suitable length of time is necessary to achieve the best results.[45] The relationship between the degradation proficiency of the catalyst for MB dye degradations and the contact time was examined at the optimized conditions of MB at pH 10, dye concentration of 10 mg/L, and catalyst dose of 0.6 g/L. The results are shown in Figure 10. The degradation of MB shows a consistent reduction with increasing irradiation time under sunlight. The decolorization of the dye solution took place in 160 min of irradiation. The corresponding degradation proficiency of MB was found to be 78.3 and 97.8% by NiO NPs and Cu−NiO NCs, respectively.

3.4.4. Effect of Catalyst Dose. The effect of photocatalyst mass on dye degradation was studied, keeping other experimental conditions constant. The percentage degradation of MB was studied under different catalyst amounts in the range of 20−60 mg at a constant dye concentration of 10 mg/

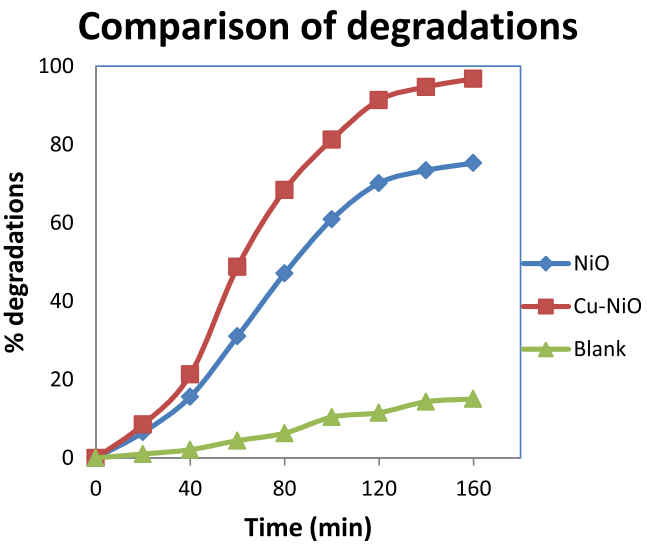

Figure 10. Comparison of degradation of MB by sunlight with and without catalysts.

L, which is in line with and lower in dose compared with a literature study.[48] The number of photons absorbed and the number of dye molecules degraded were increased with the increase in catalyst concentration.[3] The photocatalytic activity goes on increasing with catalytic load due to the uniform dispersion of the catalyst and the availability of more active sites on the surface of the catalyst.[6] Similarly, it is observed that the initial rate increases with the increase in catalyst concentration, as shown in Figure 11.

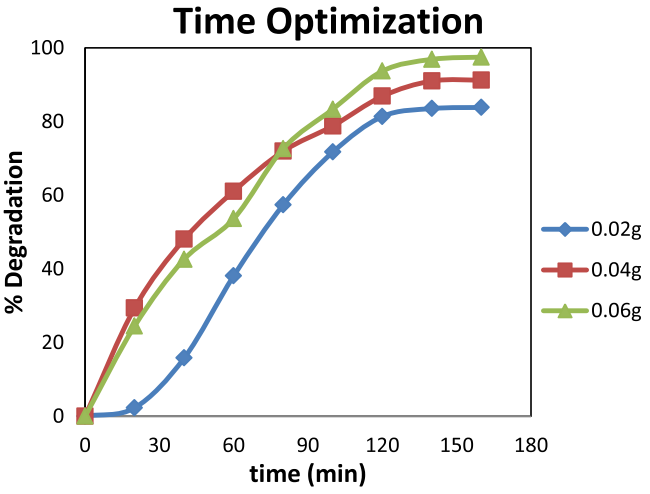

Figure 11. Effect of the irradiation time and catalyst dose on photocatalytic degradation.

3.4.5. Mechanism of Photocatalytic Degradation. When a photon of suitable energy equal to or more than the band gap interacts with the photocatalyst particle, an electron is excited from its valence band (VB) to the conduction band (CB), leaving behind a positively charged hole (h^+) at the VB, which is an electron-deficient species (Figure 12). These charge carriers (electron−hole pair) can either recombine or may involve in a series of redox reactions. The hole (h^+) may also interact with OH^- ions or a H_2O molecule to produce a highly reactive $^{\bullet}OH$ radical. At the same time, the excited electrons are gathered more at the CB, which are electron-rich species.

https://doi.org/10.1021/acsomega.2c04042
ACS Omega 2022, 7, 44720−44732

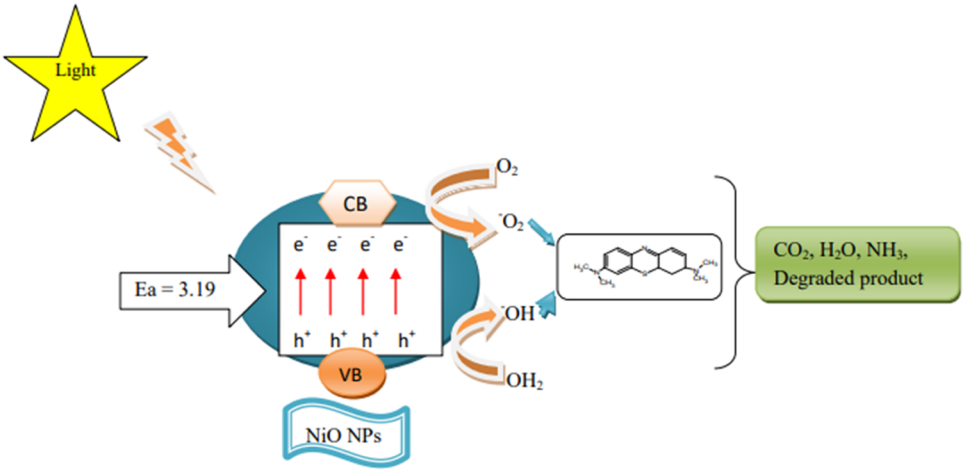

Figure 12. Photocatalytic degradation mechanism of NiO nanoparticles.

The electron at the CB reacts with the surface-adsorbed O_2 molecule to form a superoxide radical ($O_2^{-\bullet}$) that subsequently with H^+ ions through a series of steps generates a $HO_2^\bullet$ radical, H_2O_2, and then a hydroxyl radical ($^\bullet OH$). These created intermediates are highly reactive as well as strongly oxidizing in nature and oxidizes the MB dye into CO_2, H_2O, and degradation products.

3.4.6. Reusable Performance of the Nanoparticles. Reusability of a photocatalyst is very important to evaluate its efficiency. After completion of the degradation process, the catalyst was collected from the reaction medium and further used for a reusability study. To collect the catalyst, the degraded solution was centrifuged at 3000 rpm and the supernatant solution was discarded. Then, the precipitate was thoroughly washed thrice with a 3:1 water/ethanol mixture to remove the pollutant. The obtained precipitate was washed and dried at 80 °C to remove the moisture content and impurities present in the catalyst. The photocatalyst was exposed to solar light radiation for 160 min for photocatalysis. The concentrations of degraded dyes were measured using a UV−vis spectrophotometer from 5 mL of the dye solutions extracted in the prescribed time intervals. Figure 13 shows that the removal of the MB by the NiO NP and Cu−NiO NC photocatalysts after the first run achieved up to 65.08 and 70.99%. respectively. After the second run, the removal of the MB decreased down to 41.81 and 55.42%, respectively. The slight decrease in the degradation of the MB was observed in repeated runs for the photocatalytic reaction, which reveals that Cu−NiO nanocomposites have good stability and reusability performance and can be a potential candidate for practical photocatalysis applications.[3] The photocatalytic degradation of the dye was done three times. Photocatalytic activity is strongly dependent on parameters such as pH, reaction time, catalyst dose, and dye concentrations. The slight decrease in the performance of the photocatalyst may be due to the adsorption of intermediate species produced during the photodegradation of dyes onto active sites at the surface and may also be due to the photocorrosion of the catalyst.

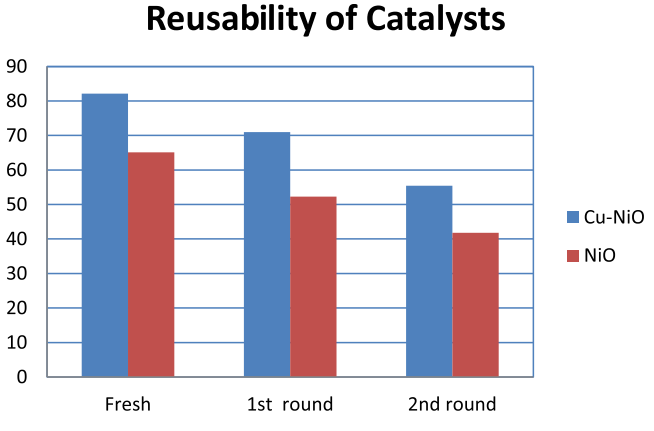

Figure 13. Reusability of the catalyst for methylene blue degradation.

The error factor because of continuous elimination of the pollutant sample during the reaction was calculated, and the error bar is indicated in Figure 14

$$\text{error factor} = \exp\left(1.96 \times \sqrt{\frac{1}{5}}\right)$$

where 1.96 is constant for 95% CI. Error factor = 2.4.

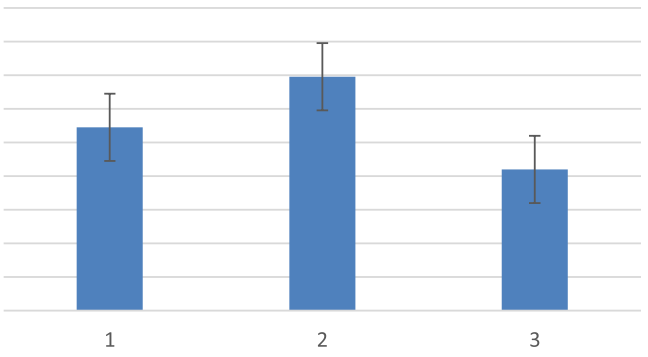

Figure 14. Error bar for NiO catalysts.

3.5. Antioxidant Activity. Antioxidants are characterized by the capacity to scavenge free radicals, and the major feauture of antioxidants is their ability to donate hydrogen or electrons to the oxidants.[6] The scavenging activities of the particles were estimated using the following concentrations: 1000, 750, 500, 250, 100, and 50 μg/mL. The results (Figure 15) showed the effective free radical scavenging activity of the synthesized samples compared to ascorbic acid (302.74 μg/mL), with calculated IC_{50} values of 350.29 and 363.96 μg/mL for Cu−NiO NCs and NiO NPs, respectively, which is in line

https://doi.org/10.1021/acsomega.2c04042
ACS Omega 2022, 7, 44720−44732

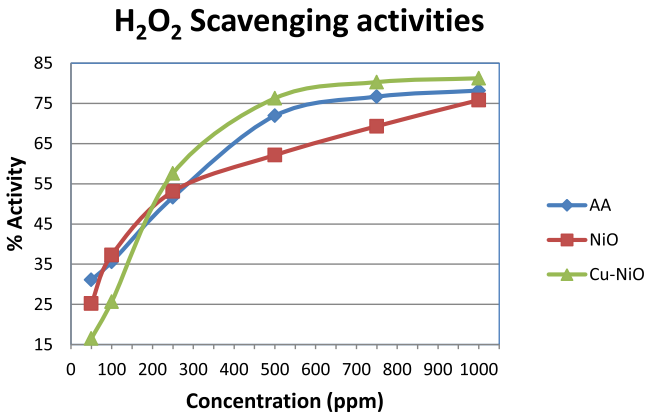

Figure 15. H_2O_2 scavenging activities of NiO and Cu−NiO nanoparticles.

with a literature study[49] that reported an IC_{50} of 339 μg/mL by biosynthesis of iron oxide (Fe_2O_3) nanoparticles. Similarly, the hydroxyl radical scavenging activity of NiO NPs (IC_{50} value is 329.20 μg/mL) is in agreement with a result reported in the literature.[6] The IC_{50} values demonstrate the ability to inhibit radicals. The result may be due to the presence of polyphenols. Phenols are the most common secondary metabolites in the plant kingdom. They have numerous biological properties including antioxidant capacities for which they are indicated in the management of several diseases.[50]

Enhancement of the antioxidant activity of the biosynthesized NiO NPs might be an effect of metal ions present in the particles. It has been reported that enzymes utilizing a metal ion (Zn) as a cofactor scavenge H_2O_2 free radicals.[51] In this study, the presence of Ni and Cu ions in particles might be responsible for the higher H_2O_2 free radical scavenging activity. The hydroxyl radical scavenging potential of NCs was found to be more significant than that of NPs.

4. CONCLUSIONS AND RECOMMENDATION

4.1. Conclusions. In general, a simple, clean, economically viable, and green approach has been established for the synthes of NiO NPs and Cu−NiO NCs using *P. dodecandra* L′Herit leaf extract as a reducing and capping agent. The UV−vis absorption peaks at 350 and 356 nm indicate the synthesis of NiO NPs and Cu−NiO NCs, respectively. FT-IR studies confirmed the biofabrication of the NPs by the action of different phytochemicals with different functional groups present in the leaf extract. The XRD patterns confirmed the purity, phase composition, and crystalline nature of the synthesized nanoparticles. The XRD pattern showed distinctive peaks corresponding to the (111), (200), (202), (311), and (222) planes that can be indexed as the typical face-centered cubic structure. Crystallite sizes of the formed particle were obtained to be 14.18 and 16.10 nm from the XRD data using the Scherrer formula for NiO NPs and Cu−NiO NCs, respectively. SEM results also demonstrate that particles are appropriately dispersed, cubical, and highly crystalline with a size of less than 10 nm. The designed nanoparticles are highly stable and show significant photocatalytic and antioxidant activities against methylene blue degradation and hydrogen peroxide scavenging. The photocatalytic degradation of methylene blue (MB) was found to be 78.3 and 97.8% by NiO NPs and Cu−NiO NCs, respectively. In the antioxidant test, NiO NPs and Cu−NiO NCs prevented the oxidation of 50% of the H_2O_2 molecules at a concentration of 363.96 and 350.29 μg/mL, respectively. Considering the obtained results, NiO NPs and Cu−NiO NCs containing *P. dodecandra* L′Herit leaf aqueous extract may be utilized as an efficient drug/supplement in treating diseases in humans after sufficient clinical studies. From the photocatalytic studies, the synthesized samples are found to be promising photocatalysts in the abatement of organic pollutants. This study offers a green and nontoxic method to synthesize nanomaterials using an eco-friendly preparation route, and it highlights the achievements in the field of photocatalysis, which is beneficial for the future work in industrial applications.

4.2. Recommendation. Advanced studies should be carried out using other additional characterization techniques which were not addressed in this study. Also, the antioxidant activity of the synthesized samples should be compared with the leaf extract.

AUTHOR INFORMATION

Corresponding Author

Ahmed Awol Yimer − *Department of Chemistry, College of Natural Sciences, Jimma University, Jimma 251, Ethiopia;* orcid.org/0000-0002-9528-8400; Email: ahmed.awol1@ju.edu.et

Authors

Soruma Gudina Firisa − *Department of Chemistry, College of Natural Sciences, Jimma University, Jimma 251, Ethiopia*

Guta Gonfa Muleta − *Department of Chemistry, College of Natural Sciences, Jimma University, Jimma 251, Ethiopia*

Complete contact information is available at: https://pubs.acs.org/10.1021/acsomega.2c04042

Notes

The authors declare no competing financial interest.

ACKNOWLEDGMENTS

The authors are highly thankful to Jimma University for its financial support.

REFERENCES

(1) Din, M. I.; Rani, A. Recent Advances in the Synthesis and Stabilization of Nickel and Nickel Oxide Nanoparticles: A Green Adeptness. *Int. J. Anal. Chem.* **2016**, *2016*, No. 3512145.

(2) Roopan, S. M.; Elango, G.; Priya, D. D.; Asharani, I. V.; Kishore, B.; et al. Sunlight Mediated Photocatalytic Degradation of Organic Pollutants by Statistical Optimization of Green Synthesized NiO NPs as Catalyst. *J. Mol. Liq.* **2019**, *293*, No. 111509.

(3) Khairnar, S. D.; Shrivastava, V. S. Facile Synthesis of Nickel Oxide Nanoparticles for the Degradation of Methylene Blue and Rhodamine B Dye: A Comparative Study. *J. Taibah Univ. Sci.* **2019**, *13*, 1108−1118.

(4) Haq, S.; Dildar, S.; Ali, M.; Ben; Mezni, A.; Hed, A.; Shahzad, M. I. Antimicrobial and Antioxidant Properties of Biosynthesized of NiO Nanoparticles Using Raphanus Sativus (R. Sativus) Extract. *Mater. Res. Express* **2021**, *8*, No. 055006.

(5) Khalil, I.; Yehye, W. A.; Etxeberria, A. E.; Alhadi, A. A.; Dezfooli, S. M.; Binti, N.; Julkapli, M. Nanoantioxidants: Recent Trends in Antioxidant Delivery Applications. *Antioxidants* **2019**, *9*, No. 24.

(6) Kumar, M. S. S.; Soundarya, T. L.; Nagaraju, G.; Raghu, G. K.; Rekha, N. D.; Alharthi, F. A.; Nirmala, B. Multifunctional Applications of Nickel Oxide (NiO) Nanoparticles Synthesized by Facile Green Combustion Method Using Limonia Acidissima Natural Fruit Juice. *Inorg. Chim. Acta* **2020**, *515*, No. 120059.

(7) Rashid, M. A. M.; Rahman, M.; Mahmud, A. O.; Morshed, A. S. M.; Haque, M. M.; Hossain, M. M. UV-Vis Spectrophotometer as an Alternative Technique for the Determination of Hydroquinone in Vinyl Acetate Monomer. *Photochem* **2022**, *2*, 435−447.
(8) Habtemariam, A. B.; Oumer, M. Plant Extract Mediated Synthesis of Nickel Oxide Nanoparticles. *Mater. Int.* **2020**, *2*, 205−209.
(9) Getu, Z. Green Synthesis and Nanoparticles Using Endod (Phytolacca dodecandra) Leaf Extract and Evaluation Of antimicrobial activities. *J. King Saud Univ. − Sci.* **2019**, *32*, 2358−2364.
(10) Sabir, F.; Bekele, E.; Gonfa, B.; Edossa, G.; Adino, A. Synthesis of Cobalt Oxide Nanoparticles Through Chemical and Biological Pathways for Antibacterial Activity. *J. Nanostructures* **2021**, *11* (3), 577−587.
(11) Srihasam, S.; Thyagarajan, K.; Korivi, M.; Lebaka, V. R.; Mallem, S. P. R. Phytogenic Generation of NiO Nanoparticles Using Stevia Leaf Extract and Evaluation of Their In-Vitro Antioxidant and Antimicrobial Properties. *Biomolecules* **2020**, *10*, No. 89.
(12) Khalil, A. T.; Ovais, M.; Ullah, I.; Ali, M.; Khan, Z.; Hassan, D.; Maaza, M.; Talha, A.; Ovais, M.; Ullah, I.; et al. Sageretia Thea (Osbeck.) Modulated Biosynthesis of NiO Nanoparticles and Their in Vitro Pharmacognostic, Antioxidant and Cytotoxic Potential. *Artif. Cells, Nanomed., Biotechnol.* **2018**, *46*, 838−852.
(13) Ezhilarasi, A. A.; Vijaya, J. J.; Kaviyarasu, K.; Zhang, X.; Kennedy, L. J. Green Synthesis of Nickel Oxide Nanoparticles Using Solanum Trilobatum Extract for Cytotoxicity, Antibacterial and Photocatalytic Studies. *Surf. Interfaces* **2020**, *20*, No. 100553.
(14) Arun, L.; Karthikeyan, C.; Philip, D.; Unni, C. Journal of Physics and Chemistry of Solids Optical, Magnetic, Electrical, and Chemo-Catalytic Properties of Bio- Synthesized CuO / NiO Nanocomposites. *J. Phys. Chem. Solids* **2020**, *136*, No. 109155.
(15) Gebreslassie, H. B.; Eyasu, A. Phytochemical Screening of the Leaves Calpurnia Aurea (Ait.) Benth Extract. *Int. J. Clin. Chem. Lab. Med.* **2019**, *5*, 18−24.
(16) Ganesan, K.; Kumar, S.; Nair, P.; Letha, N.; Banu, G.Phytochemical Screening of Different Solvent Extracts of Soap Berry (Phytolacca dodecandra L' Herit.) - A Native Ethiopian Shrub, 2016.
(17) Amita; Deepak; Arun; Rana, P. S. Synthesis, Characterization and Sunlight Catalytic Performance of Cu Doped NiO Nanoparticles. *AIP Conf. Proc.* **2019**, *2093*, No. 020035.
(18) Ahmad, Z.; Afzal, A. M.; Khan, M. F.; Manzoor, A.; Khalil, H. M. W.; Aftab, S. Copper-Doped Nickle-Oxide Nanoparticles for Photocatalytic Degradation of Erichrome Black-T and Methylene Blue and Its Solar Cell Applications. *J. Nanoelectron. Optoelectron.* **2019**, *14*, 1304−1312.
(19) Patil, S.; Rajiv, P.; Sivaraj, R.An investigation of antioxidant and cytotoxic properties of green synthesized silver nanoparticles*Indo Am. J. Pharm. Sci.***2015**.
(20) Abbasi, B. A.; Iqbal, J.; Mahmood, T.; Ahmad, R.; Kanwal, S. Plant-Mediated Synthesis of Nickel Oxide Nanoparticles (NiO) via Geranium Wallichianum: Characterization and Different Biological Applications. *Mater. Res. Express* **2019**, *6*, No. 0850a7.
(21) Khan, S. A.; Shahid, S.; Ayaz, A.; Alkahtani, J.; Elshikh, M. S.; Riaz, T. Phytomolecules-Coated NiO Nanoparticles Synthesis Using Abutilon Indicum Leaf Extract: Antioxidant, Antibacterial, and Anticancer Activities. *Int. J. Nanomed.* **2021**, *16*, 1757−1773.
(22) Rajendaran, K.; Muthuramalingam, R.; Ayyadurai, S. Green Synthesis of Ag-Mo/CuO Nanoparticles Using Azadirachta Indica Leaf Extracts to Study Its Solar Photocatalytic and Antimicrobial Activities. *Mater. Sci. Semicond. Process.* **2019**, *91*, 230−238.
(23) Das, S. S.; Lucas, D. T.; Sica, D. A.; Cássia, R. H.; Luciano, B. M.; Taylor, S.; et al. Controlled initial surge despite high drug fraction and high solubility. *Pharm. Dev. Technol.* **2017**, *22*, 35−44.
(24) Christopher, J. G.; Saswati, B.; Ezilrani, P. Optimization of Parameters for Biosynthesis of Silver Nanoparticles Using Leaf Extract of Aegle Marmelos. *Braz. Arch. Biol. Technol.* **2015**, *58*, 702−710.
(25) Meva, F. M.; Okalla, C.; Antoinette, A.; Belle, P.; Kedi, E.; Deli, V.; Etoh, M.; Mpondo, E.; et al. Spectroscopic Synthetic Optimizations Monitoring of Silver. *Rev. Bras. Farmacogn.* **2016**, *26*, 640−646.
(26) Skiba, M. I.; Vorobyova, V. I. Synthesis of Silver Nanoparticles Using Orange Peel Extract Prepared by Plasmochemical Extraction Method and Degradation of Methylene Blue under Solar Irradiation. *Adv. Mater. Sci. Eng.* **2019**, *2019*, 1−8.
(27) Adewale, S. A.; Similoluwa, A.; Adekunle, F.; Kolawole, A. Heliyon Green Synthesis of Copper Oxide Nanoparticles for Biomedical Application and Environmental Remediation. *Heliyon* **2020**, *6*, No. e04508.
(28) Letchumanan, D.; Sok, S. P. M.; Ibrahim, S.; Nagoor, N. H.; Arshad, N. M. Plant-Based Biosynthesis of Copper / Copper Oxide Nanoparticles: An Update on Their Applications in Biomedicine Mechanisms and Toxicity. *Biomolecules* **2021**, *11*, 564.
(29) Bukhari, S. I.; Hamed, M. M.; Al-agamy, M. H.; Gazwi, H. S. S.; Radwan, H. H.; Youssif, A. M. Biosynthesis of Copper Oxide Nanoparticles Using Streptomyces MHM38 and Its Biological Applications. *J. Nanomater.* **2021**, *2021*, 1−16.
(30) Hulkoti, N. I.; Taranath, T. C. Biosynthesis of Nanoparticles Using Microbes-A Review. *Colloids Surf., B* **2014**, *121*, 474−483.
(31) Chen, M. N.; Chan, C. F.; Huang, S. L.; Lin, Y. S. Green Biosynthesis of Gold Nanoparticles Using Chenopodium Formosanum Shell Extract and Analysis of the Particles' Antibacterial Properties. *J. Sci. Food Agric.* **2019**, *99*, 3693−3702.
(32) Sheo, L.; Upadhyay, B.; Kumar, N. Green Synthesis of Copper Nanoparticle Using Glucose and Polyvinylpyrrolidone (PVP). *Inorg. Nano-Met. Chem.* **2017**, *47*, 1436−1440.
(33) Gnanaprakasam, A.; Sivakumar, V. M.; Thirumarimurugan, M. A Study on Cu and Ag Doped ZnO Nanoparticles for the Photocatalytic Degradation of Brilliant Green Dye: Synthesis and Characterization. *Water Sci. Technol.* **2016**, *74*, 1426−1435.
(34) Haider, A.; Ijaz, M.; Ali, S.; Haider, J.; Imran, M.; Majeed, H.; Shahzadi, I.; Ali, M. M.; Khan, J. A.; Ikram, M. Green Synthesized Phytochemically (Zingiber Officinale and Allium Sativum) Reduced Nickel Oxide Nanoparticles Confirmed Bactericidal and Catalytic Potential. *Nanoscale Res. Lett.* **2020**, *15*, 50.
(35) Khan, S. A.; Shahid, S.; Ayaz, A.; Alkahtani, J.; Elshikh, M. S.; Riaz, T. Phytomolecules-Coated NiO Nanoparticles Synthesis Using Abutilon Indicum Leaf Extract: Antioxidant, Antibacterial, and Anticancer Activities. *Int. J. Nanomed.* **2021**, *16*, 1757−1773.
(36) Uddin, S.; Safdar, L.; Anwar, S.; Iqbal, J.; Laila, S.; Abbasi, B. A.; Saif, M. S.; Ali, M.; Rehman, A.; Basit, A.; et al. Green Synthesis of Nickel Oxide Nanoparticles from Berberis Balochistanica Stem for Investigating Bioactivities. *Molecules* **2021**, *26*, No. 1548.
(37) Varunkumar, K.; Hegde, G.; Ethiraj, A. S.; et al. Materials Science in Semiconductor Processing E Ff Ect of Calcination Temperature on Cu Doped NiO Nanoparticles Prepared via Wet-Chemical Method: Structural, Optical and Morphological Studies. *Mater. Sci. Semicond. Process.* **2017**, *66*, 149−156.
(38) Kumar, J. K.; Prasad, A. G. D. Identification and Comparison of Biomolecules in Medicinal Plants of Tephrosia Tinctoria. *Rom. J. Biophys* **2011**, *21*, 63−71.
(39) Komal Kumar, J.; Devi Prasad, A. G. Identification and Comparison of Biomolecules in Medicinal Plants of Tephrosia Tinctoria. *Rom. J. Biophys.* **2011**, *21*, 63−71.
(40) Zahra, T.; Ahmad, K. S. Optik Structural, Optical and Electrochemical Studies of Organo-Templated Wet Synthesis of Cubic Shaped Nickel Oxide Nanoparticles. *Optik* **2020**, *205*, No. 164241.
(41) Zhang, Q.; Xu, S.; Li, Y.; Ding, P.; Zhang, Y.; Zhao, P. Green-Synthesized Nickel Oxide Nanoparticles Enhances Biohydrogen Production of Klebsiella Sp. WL1316 Using Lignocellulosic Hydrolysate and Its Regulatory Mechanism. *Fuel* **2021**, *305*, No. 121585.
(42) Said, A. E.-A. A.; El-wahab, M. M. A.; Soliman, S. A.; Goda, M. N. Synthesis and Characterization of Nano CuO-NiO Mixed Oxides. *Nanosci. Nanoeng.* **2014**, *2*, 17−28.
(43) Said, A. E.-A.; El-Wahab, M. M.A.; Soliman, S. A.; Goda, M. N. Synthesis and Characterization of Nano CuO-NiO Mixed Oxides. *Nanoscience and Nanoengineering* **2014**, *2*, 17−28.

https://doi.org/10.1021/acsomega.2c04042
ACS Omega 2022, 7, 44720−44732

(44) Ghazal, S.; Khandannasab, N.; Ali, H.; Sabouri, Z.; Rangrazi, A.; Darroudi, M. Green Synthesis of Copper-Doped Nickel Oxide Nanoparticles Using Okra Plant Extract for the Evaluation of Their Cytotoxicity and Photocatalytic Properties. *Ceram. Int.* **2021**, *47*, 27165−27176.
(45) Hameeda, B. B.; Mushtaq, A.; Saeed, M.; Munir, A.; Waseem, A. Development of Cu-Doped NiO Nanoscale Material as Efficient Photocatalyst for Visible Light Dye Degradation. *Toxin Rev.* **2020**, *40*, 1396−1406.
(46) Karthikeyan, M.; Kumar, P. V.; Ahamed, A. J.; Ravikumar, A. Synthesis of Mg^{2+} Doped NiO Nanoparticles and Their Structural and Optical Properties by Co-Precipitation Method. *J. Adv. Appl. Sci. Res.* **2014**, *2*, 1−9.
(47) Agale, A. A.; Gaikwad, S. T.; Rajbhoj, A. S. Nanosized Synthesis of Nickel Oxide by Electrochemical Reduction Method and Their Antifungal Screening. *J. Cluster Sci.* **2017**, *28*, 2097−2109.
(48) Ezhilarasi, A. A.; Vijaya, J. J.; Kaviyarasu, K.; Kennedy, L. J.; Ramalingam, R. J.; Al-lohedan, H. A. Green Synthesis of NiO Nanoparticles Using Aegle Marmelos Leaf Extract for the Evaluation of in-Vitro Cytotoxicity, Antibacterial and Photocatalytic Properties. *J. Photochem. Photobiol. B* **2018**, *180*, 39−50.
(49) Khalil, A. T.; Ovais, M.; Ullah, I.; Ali, M.; Khan, Z.; Maaza, M.; Talha, A.; Ovais, M.; Ullah, I.; Ali, M. Green Chemistry Letters and Reviews Biosynthesis of Iron Oxide (Fe_2O_3) Nanoparticles via Aqueous Extracts of Sageretia Thea (Osbeck.) and Their Pharmacognostic Properties. *Green Chem. Lett. Rev.* **2017**, *10*, 186−201.
(50) Iteku, J. B.; Mbayi, O.; Bongo, G. N.; Mutwale, P. K.; Wambale, J. M.; Lengbiye, E.; Inkoto, C. L.; Ngunde, S. N.; Ngbolua, K. Phytochemical Analysis and Assessment of Antibacterial and Antioxidant Activities of Phytolacca Dodecandra L. Herit Leaf Extracts (Phytolaccaceae). *Int. J. Biomed. Eng. Clin. Sci.* **2019**, *5*, 31−39.
(51) Umar, H.; Kava, D.; Rizaner, N. Biosynthesis of Zinc Oxide Nanoparticles Using Albizia Lebbeck Stem Bark, and Evaluation of Its Antimicrobial, Antioxidant, and Cytotoxic Activities on Human Breast Cancer Cell Lines. *Int. J. Nanomed.* **2019**, *14*, 87−100.

https://doi.org/10.1021/acsomega.2c04042
ACS Omega 2022, 7, 44720−44732